# Sliding Mode Control (SMC) of PWM Dual Inverter Based Grid Connected PV System: Modelling and Performance analysis

Nayan Kumar, Tapas Kumar Saha, *Member, IEEE* and Jayati dey, *Member, IEEE*

***Abstract*—This paper proposes a novel robust & adaptive sliding mode (SM) control for a cascaded two-level inverter (CTLI)-based grid connected photovoltaic (PV) system. The modelling and design of the control scheme for the CTLI-based grid connected PV system is developed to supply active power and reactive power with variable solar irradiance. A vector controller is developed keeping the maximum power delivery of the PV in consideration. Two different switching schemes have been considered to design SM controllers and studied under similar operating situations. Instead of the referred space vector PWM technique, a simple PWM modulation technique is used for the operation of the proposed SM controller. The performance of the SM controller is improved by using an adaptive hysteresis-band (HB) calculation. The controller performance is found to be satisfactory for both the schemes at considered load and solar irradiance level variations in simulation environment. The laboratory prototype, operated with the proposed controller is found to be capable of implementing the control algorithm successfully in the considered situation.**

***Index Terms*—Photovoltaic (PV) system, multilevel inverter, Vector control, sliding mode control (SMC), distribution static compensator (Distribution-STATCOM)**

NOMENCLATURE

$V$ = Solar cell terminal voltage [V]
$I$ = Solar cell terminal current [A]
$I_{ph}$ = Photo generated current [linear with irradiance]
$I_s$ = Saturation current due to diffusion mechanism
$T$ = Cell temperature [K]
$K$ = Boltzmann's constant
$q$ = Electron charge
$n$ = Diode quality factor [silicon diode $n$ =2]
$R_s$ =Cell series resistance [Ω]
$R_{sh}$ = Cell shunt resistance [Ω]
$N_P$ = Number of parallel cells
$N_s$ = Number of series cells
$V_{dc}$ = dc-link voltage of the voltage source inverter (VSI)
$V_a$, $V_b$, $V_c$ = Per phase grid voltages
$e_{a1}$, $e_{b1}$, $e_{c1}$ = First inverter pole voltages
$e_{a2}$, $e_{b2}$, $e_{c2}$ = Second inverter pole voltages
$V_q$ = q-component of the source voltage
$V_d$ = d-component of the source voltage

Manuscript received April 1, 2015; revised Jun 27, 2015 and October 5, 2015; accepted October 18, 2015. Recommended for publication by Associate Editor xxxx

The authors are with the Electrical Engineering Department, National Institute of Technology, Durgapur-713209, India
(e-mail: nayansays@gmail.com, tapassahanit@gmail.com and deybiswasjayati@gmail.com)

## I. INTRODUCTION

IN recent years, the grid connected PV system is becoming popular, because of rapidly increasing energy demand and the environmental impacts of fossil fuel based energy supply. Many developing countries have permitted, encouraged, and even funded the integration of renewable energy source into the electrical grid. It has been shown in [1]-[3] the novel power-electronic technology plays a very crucial role in the distributed generation (DG) and electrical grid tie of renewable energy sources (PV system, wind energy etc.). Some PV systems, using power conversion for grid interfacing have been proposed in [1], [3]-[5].The multilevel voltage-source converters have emerged as one of the preferred choices for medium voltage (MV) high-power applications due to several advantages [6], [7]. Some of the most popular topologies of multilevel voltage-source converters are neutral-point or diode-clamped converters (NPC), flying-capacitor (FC) converters and cascaded H-Bridge converters (CHB) [5], [7], [8]. The cascaded H-bridge converter receives large attention among these topologies, due to the modular circuit layout [9]-[11]. The major advantage of CHB over other topologies is a minimal requirement of dc sources; the number of levels in the output voltage can be increased. The merit of CTLI-based grid connected PV system is reduced current and voltage harmonics. Moreover, the $dv/dt$ stress is reduced, which is very important for high-power applications and higher redundant switching state combinations, compared to single-inverter for same output voltage levels [5], [12]. In [5] isolated CTLI in low frequency are used. The CTLI topology associated with line-frequency transformer has been proposed in [5], [9], and [11]-[13]. In the present study, also line frequency transformers are used at the output of the PV supplied CTLI.

Various control strategies are available in literature to control the converters, incorporating the space vector modulation (SVM) [10] and a PWM with phase-shifted carriers within each H-bridge of each multilevel phase leg



2168-6777 (c) 2015 IEEE. Personal use is permitted, but republication/redistribution requires IEEE permission. See http://www.ieee.org/publications_standards/publications/rights/index.html for more information.

[14]. However, one of the robust and dynamic control techniques is the sliding mode control (SMC). This control is a kind of nonlinear control, which has been developed primarily for the control of variable structure systems (VSS). Nowadays, SMC is used because of its several advantages [15]-[20]. Such properties make SMC highly suitable for applications in power converters and their wide utilization in industrial applications, e.g., electrical drives, high-voltage and high-power applications, which require multilevel inverters or parallel inverters [5], [20] as VSIs, dc-dc converters [15], [18] etc. The SM control suffers from chattering problem, which leads to variable and high frequency switching in the converter. This phenomenon increases power losses and also produces severe electromagnetic compatibility (EMC) noise. The chattering effect is controllable through the level of the hysteresis band in the hysteresis modulator of the SM controller [15], [18].

In the literature, CTLI topology has been proposed for different applications [5], [6], [9], [11]-[13] and [21]. This paper, deals with the modelling of the CTLI based grid connected photovoltaic system. The SMC is proposed for control of the output currents of this CTLI. The control of the capacitor voltage is developed using a vector control scheme. In this work, the PV modules are designed to produce a dc voltage of 48 V under rated Indian solar irradiance. The inverter, however, is connected with a distribution grid of three-phase ac 400 V (line to line). The circuit-based model of a PV array that can be implemented in any simulation environment is proposed in [22], [24]-[26]. In the present study, single diode model of solar cell is used following the mathematical model developed in [22], [23].

The Photovoltaic systems are connected to the CTLI, and inverter output to the low voltage (LV) side of an open winding three-phase transformer. The complete power scheme is shown in Fig. 1.

The paper discusses the problem with following contributions:

i) Two isolated PV sources are designed to supply active power at 48 V at a normal Indian solar irradiance. This ensures the maximum power delivery of the system at rated condition.
ii) A novel SM control scheme is proposed so that the CTLI based system would work under variable solar irradiance levels and also in the absence of solar irradiance (as Distribution STATCOM).
iii) The controllers are designed and tested for two different switching schemes, *a) Two-Level Switching and b) Forced Switching.*
iv) To improve the performance of SMC, the present work develops a systematic adaptive procedure to calculate the band of the hysteresis comparators.
v) The input solar irradiance is varied and also reduced to zero to establish the operation of the control with variable level of active power supply and reactive power supply.
vi) The modulation technique for the CTLI is established with a simple PWM technique instead of referring Space Vector modulation technique.
vii) The CTLI based power supply using the proposed SMC is tested in real time standalone mode through a laboratory prototype.

The paper is organized as follows: In Section II presents a mathematical model grid connected PV system. The system configuration is given in Section III. Simulation results followed by discussion are presented in Section IV. It also describes the experimental system and results for the real time implementation of SMC. Finally, the conclusions that have been drawn from the present work are summarized in Section V.

## II. MATHEMATICAL MODELLING OF THE SYSTEM

The characteristic equation of PV cells is given by (1)

$$I = I_{ph} - I_s\left[\exp\frac{q(V+IR_S)}{nKT} - 1\right] - \frac{V+R_S I}{R_{sh}} \quad (1)$$

The equivalent circuit determined from the equation is used for the simulation model, is shown in Fig. 2.

The parameter values are $R_s = 0.4\Omega, R_{sh} = 323\Omega$. If a string has $M$ identical modules, $N$ identical PV strings can be in parallel to build a PV array containing $(M \times N)$ PV modules.

The complete multidimensional array model equation is shown in (2).

$$I = N_p\left[I_{ph} - I_s\left(\exp\frac{q\left[\left(\frac{V}{N_s}\right)+\left(\frac{I}{N_p}\right)R_s\right]}{KT} - 1\right) - \frac{\left(\frac{V}{N_s}\right)+\left(\frac{I}{N_p}\right)R_s}{R_{sh}}\right] \quad (2)$$

The number of cells connected in series to form one set, and the number of sets connected in parallel to form one array has been considered to provide maximum power at 48 V at the normal Indian solar irradiance.

Power rating of the inverter is taken as 2.5 kW The available output power at different output voltage is shown in Fig. 3. Here the output power is found to be maximum at 48 V with fixed solar irradiance.

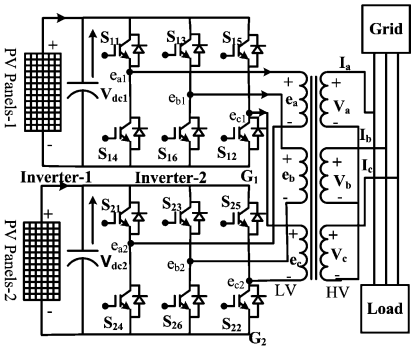


Fig. 1. Power circuit of the photovoltaic system with cascaded two-level inverter

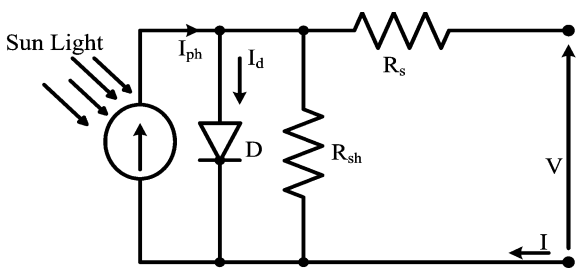


Fig.2. Equivalent circuit of PV cell

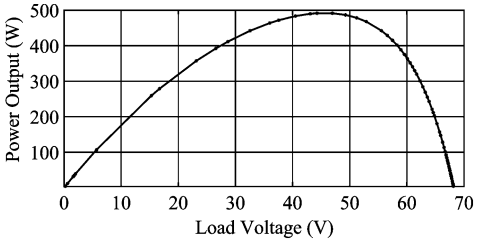


Fig. 3. Power-Voltage characteristics for the PV system

Accordingly, the controllers are designed to maintain the total PV output voltage of the two inverters (as shown in Fig. 1) at 96 V, to ensure maximum power delivery by the system.

### A. CTLI model

For the considered power scheme, the voltage across *a*, *b* and *c* windings are as follows:

$$e_a = \frac{2}{3}(e_{a1} - e_{a2}) - \frac{1}{3}(e_{b1} - e_{b2}) - \frac{1}{3}(e_{c1} - e_{c2}) \tag{3}$$

$$e_b = -\frac{1}{3}(e_{a1} - e_{a2}) + \frac{2}{3}(e_{b1} - e_{b2}) - \frac{1}{3}(e_{c1} - e_{c2}) \tag{4}$$

$$e_c = -\frac{1}{3}(e_{a1} - e_{a2}) - \frac{1}{3}(e_{b1} - e_{b2}) + \frac{2}{3}(e_{c1} - e_{c2}) \tag{5}$$

Where, $e_{a1}, e_{b1}, e_{c1}$ are first inverter pole voltages and $e_{a2}, e_{b2}, e_{c2}$ are second inverter pole voltages.

Assuming ideal power switches, the output voltage of the CTLI is obtained as (3), (4) and (5) which can be rewritten in matrix form as (6).

$$\begin{bmatrix} e_a \\ e_b \\ e_c \end{bmatrix} = \frac{1}{3}\begin{bmatrix} 2 & -1 & -1 \\ -1 & 2 & -1 \\ -1 & -1 & 2 \end{bmatrix}\begin{bmatrix} e_{a_1} \\ e_{b_1} \\ e_{c_1} \end{bmatrix} - \frac{1}{3}\begin{bmatrix} 2 & -1 & -1 \\ -1 & 2 & -1 \\ -1 & -1 & 2 \end{bmatrix}\begin{bmatrix} e_{a_2} \\ e_{b_2} \\ e_{c_2} \end{bmatrix} \tag{6}$$

The design of sliding-mode control requires two conditions to be satisfied, namely, reaching and sliding phases [15]-[20]. Switching surface, which will be called here onward as switching function $s_{ij}$, is defined by the following control law:

Six switching functions $\gamma_{ij}, i \in \{1,2\}, j \in \{1,2,3\}$ can be obtained as follows

$$\gamma_{ij} = \begin{cases} 1 \text{ if } S_{ij} \text{ is ON } \overline{S_{ij}} \text{ OFF} \\ 0 \text{ if } S_{ij} \text{ is OFF } \overline{S_{ij}} \text{ ON} \end{cases} \tag{7}$$

Thus, the three- phase output voltages of the CTLI related to the switching states can be expressed as:

$$V_{k1} \in \gamma_{1j} V_{dc1}, \qquad k \in \{a,b,c\} \tag{8}$$

$$V_{k2} \in \gamma_{2j} V_{dc2}, \qquad k \in \{a,b,c\} \tag{9}$$

$$\begin{bmatrix} e_a \\ e_b \\ e_c \end{bmatrix} = \frac{1}{3}\begin{bmatrix} 2 & -1 & -1 \\ -1 & 2 & -1 \\ -1 & -1 & 2 \end{bmatrix}\begin{bmatrix} \gamma_{11} \\ \gamma_{12} \\ \gamma_{13} \end{bmatrix} V_{dc1} - \frac{1}{3}\begin{bmatrix} 2 & -1 & -1 \\ -1 & 2 & -1 \\ -1 & -1 & 2 \end{bmatrix}\begin{bmatrix} \gamma_{21} \\ \gamma_{22} \\ \gamma_{23} \end{bmatrix} V_{dc2} \tag{10}$$

### B. Vector control

The two-axis representation of the supply voltages can be formed as:

$$\begin{bmatrix} V_\alpha \\ V_\beta \end{bmatrix} = \frac{2}{3}\begin{bmatrix} 1 & -1/2 & -1/2 \\ 0 & -\sqrt{3}/2 & \sqrt{3}/2 \end{bmatrix}\begin{bmatrix} V_a \\ V_b \\ V_c \end{bmatrix} \tag{11}$$

Accordingly, (10) can be expressed as (12).

$$\begin{bmatrix} V_\alpha \\ V_\beta \end{bmatrix} = \frac{2}{3}\begin{bmatrix} 1 & -1/2 & -1/2 \\ 0 & -\sqrt{3}/2 & \sqrt{3}/2 \end{bmatrix}\begin{bmatrix} \gamma_{1\alpha} \\ \gamma_{1\gamma} \end{bmatrix} V_{dc1} - \frac{2}{3}\begin{bmatrix} 1 & -1/2 & -1/2 \\ 0 & -\sqrt{3}/2 & \sqrt{3}/2 \end{bmatrix}\begin{bmatrix} \gamma_{2\alpha} \\ \gamma_{2\gamma} \end{bmatrix} V_{dc2} \tag{12}$$

Here, $V_{dc1} = V_{dc2} = 48\text{V}$. The d-q axis of the used vector control are derived following Fig. 4, and found as:

$$\begin{bmatrix} V_d \\ V_q \end{bmatrix} = \begin{bmatrix} \sin\omega t & \cos\omega t \\ \cos\omega t & -\sin\omega t \end{bmatrix}\begin{bmatrix} V_m \sin\omega t \\ V_m \cos\omega t \end{bmatrix} \tag{13}$$

The equivalent circuit for '*a*' phase is shown in Fig. 5 in which $V_a$ is the grid voltage, $R$ is the loss representing resistance, $L$ is the leakage inductance of transformer windings, $n(e_{a1} - e_{a2})$ is the voltage across the primary of the transformer. The transformer is step-up with turn ratio *1: n.* Applying KVL for '*a*', '*b*' and '*c*' phases

$$n(e_{a1} - e_{a2}) = \mathrm{R}_a i_a + L_a \frac{di_a}{dt} + V_a \tag{14}$$

$$n(e_{b1} - e_{b2}) = \mathrm{R}_b i_b + L_b \frac{di_b}{dt} + V_b \tag{15}$$

$$n(e_{c1} - e_{c2}) = \mathrm{R}_c i_c + L_c \frac{di_c}{dt} + V_c \tag{16}$$

$R_a, R_b,$ and $R_c$ are considered to be equal to $R$ and the $L_a, L_b,$ and $L_c$ are equal to $L$. Hence,

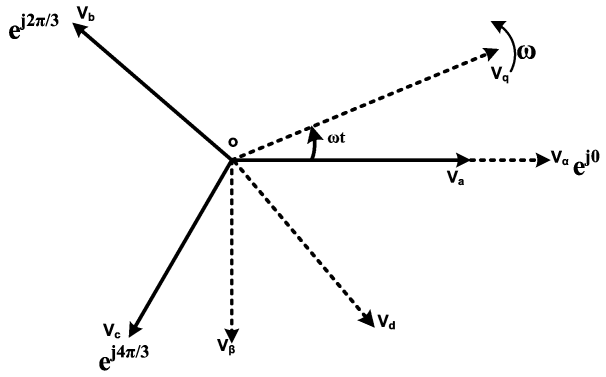


Fig.4. Vector diagram of the voltage

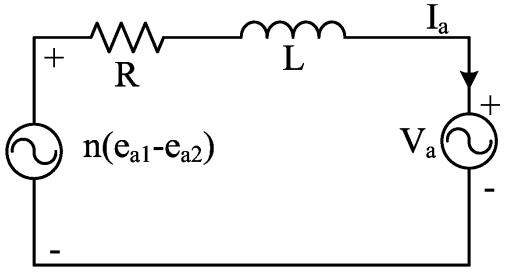


Fig.5. Single phase equivalent circuit



2168-6777 (c) 2015 IEEE. Personal use is permitted, but republication/redistribution requires IEEE permission. See http://www.ieee.org/publications_standards/publications/rights/index.html for more information.

$$\frac{d}{dt}\begin{bmatrix} i_a \\ i_b \\ i_c \end{bmatrix} = \begin{bmatrix} -R/L & 0 & 0 \\ 0 & -R/L & 0 \\ 0 & 0 & -R/L \end{bmatrix}\begin{bmatrix} i_a \\ i_b \\ i_c \end{bmatrix} + \frac{1}{3L}\begin{bmatrix} 2 & -1 & -1 \\ -1 & 2 & -1 \\ -1 & -1 & 2 \end{bmatrix}\begin{bmatrix} \gamma_{11} \\ \gamma_{12} \\ \gamma_{13} \end{bmatrix} nV_{dc1} - \frac{1}{3L}\begin{bmatrix} 2 & -1 & -1 \\ -1 & 2 & -1 \\ -1 & -1 & 2 \end{bmatrix}\begin{bmatrix} \gamma_{21} \\ \gamma_{22} \\ \gamma_{23} \end{bmatrix} nV_{dc2} + \begin{bmatrix} 1/L & 0 & 0 \\ 0 & 1/L & 0 \\ 0 & 0 & 1/L \end{bmatrix}\begin{bmatrix} -V_a \\ -V_b \\ -V_c \end{bmatrix} \quad (17)$$

Equation (17) is transformed to synchronously rotating reference frame as follows.

$$\frac{d}{dt}\begin{bmatrix} i_d \\ i_q \end{bmatrix} = \begin{bmatrix} -\frac{R}{L} & \omega \\ -\omega & -\frac{R}{L} \end{bmatrix}\begin{bmatrix} i_d \\ i_q \end{bmatrix} + \begin{bmatrix} -\frac{1}{L} & \frac{1}{L} \\ -\frac{1}{L} & \frac{1}{L} \end{bmatrix}\begin{bmatrix} \gamma_{d1} \\ \gamma_{q1} \end{bmatrix} V_{dc1} - \begin{bmatrix} -\frac{1}{L} & \frac{1}{L} \\ -\frac{1}{L} & \frac{1}{L} \end{bmatrix}\begin{bmatrix} \gamma_{d2} \\ \gamma_{q2} \end{bmatrix} V_{dc2} + \begin{bmatrix} \frac{1}{L} & 0 \\ 0 & \frac{1}{L} \end{bmatrix}\begin{bmatrix} -V_d \\ -V_q \end{bmatrix} \quad (18)$$

Where, $i_d$ , $i_q$ are d–q axes components of the cascaded inverter output current, respectively.

The dynamics of the dc-link can be represented by:

$$\frac{d}{dt}\begin{bmatrix} V_{dc1} \\ V_{dc2} \end{bmatrix} = \frac{1}{C}\left[\begin{bmatrix} \gamma_{d1} & \gamma_{q1} \\ \gamma_{d2} & \gamma_{q2} \end{bmatrix}\begin{bmatrix} i_d \\ i_q \end{bmatrix} - \begin{bmatrix} I_{dc1} \\ I_{dc2} \end{bmatrix}\right] \quad (19)$$

The reference value of d-axis current is generated from dc-link voltage controller. In this work, the reference the total of two dc voltage is kept at 96 V.

### C. Sliding mode control (SMC)

The SMC consists of a time-varying state-feedback discontinuous control law that switches at a high frequency from one continuous structure to another, according to the present position of the state variables in the state space. The objective is to force the dynamics of the system under control to follow exactly what is desired and pre-determined [15]. SMC is particularly interesting due to its known characteristics of robustness, system order reduction [15]–[20], and [28]-[30], and appropriateness to the ON–OFF behaviour of power switches. One of the most important features of the sliding mode regime, in variable structure systems (VSS), is the ability to achieve responses that are independent of the system parameters. The easy implementation of SM control through hysteresis band does not require additional computation or auxiliary circuitries. There are basically three approaches in keeping the switching frequency of the hysteresis modulation (HM)-based SM controller constant [15]. (a) Constant ramp or timing functions directly into the controller. In this control scheme the fixed switching frequency under all operating conditions, and controlled through varying the ramp/timing function. (b) Adaptive control into the HM-based SM controller to counteract the switching frequency variation. (c) Constant switching frequency SM controllers can also be obtained by employing PWM instead of HM.

This work, presents the main steps to design the SMC, applied to CTLI. A cascaded control structure with an inner current control loop and an outer voltage control loop can solve the control problem. The cascaded control structure is chosen for ease of control realization and to exploit the motion separation property of power converters. For power converters, the fast motion is dominated by the dynamics of the loop current, whereas the slow motion stems from the dynamics of the output voltage. The power converters inherently include switching devices, yielding a discontinuous control law. The voltage controls are usually realized with standard vector control techniques; whereas the current control is implemented using either sliding mode PWM or hysteresis control. Here the SM approach is applied to control the current error. The goal of the system controller is to accomplish voltage regulation of the inverter capacitors. This is accomplished by controlling the active and reactive power that flows into the grid. Due to the characteristics of SM controllers, such as fast speed of response and superior robustness to external perturbations, this controlling methodology has been adopted as an alternative to conventional one. This SMC is designed considering first a selected sliding surface and then the control law driving the state of the system onto the sliding surface. The gate signals for first and second inverters are generated following hysteresis modulation technique in the two switching schemes, which are discussed as follows.

*Two-Level Switching: Scheme-I*

In this scheme, the inverter is operated under bipolar modulation with two levels of output 1 and -1. Fig. 6 shows the switching logic. For a particular phase of the two inverters, two switches are turned on, and the other two switches are turned off, in each cycle. If $f_{sw}$ is the switching frequency, then the switching loss per on-off is proportional to the switching frequency and given by $P_{Inv} = kf_{sw}$. The total switching loss is $2P_{Inv.}$. A variable structure control ($u$) is described as

$$u = \begin{cases} +1, \ if \ S_e > +HB \\ -1, \ if \ S_e < -HB \end{cases} \quad (20)$$

where, $S_e$ is the error between the actual value of the state variable and its corresponding reference. According to SM theory, $S_K$ crosses the switching surface $(S_k)$ at every switching instant, satisfying the SM conditions. Scheme I, as discussed above, is depicted in Fig. 7.

*Forced Switching: Scheme-II*

Fig. 8 presents the schematic diagram for Scheme II. Under this scheme, prefixed switching frequency can be obtained by comparing the switching function with fixed frequency carrier signal. The carrier signal is triangular in nature. The amplitude of triangular signal is same as the hysteresis band.

The technique retains the robustness properties of hysteresis controller while achieving the constant switching frequency. Further, there is a minimum magnitude bound for the carrier signal at different frequencies.

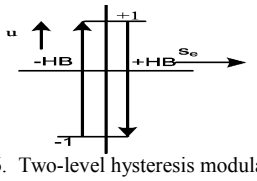


Fig. 6. Two-level hysteresis modulation



2168-6777 (c) 2015 IEEE. Personal use is permitted, but republication/redistribution requires IEEE permission. See http://www.ieee.org/publications_standards/publications/rights/index.html for more information.

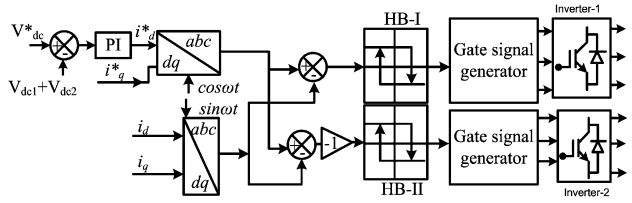


Fig.7.Control block diagram of Scheme-I

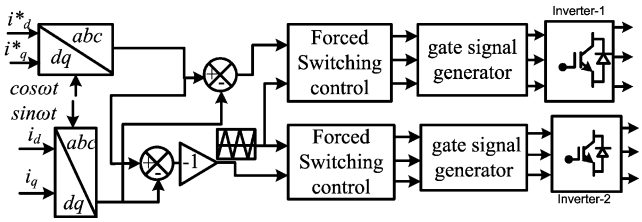


Fig.8.Control block diagram of Scheme-II

The inverter may enter into complex switching states below this magnitude. Moreover, the tracking error and settling time increase with the increase in the magnitude of the carrier. Therefore, it is essential to calculate the optimal magnitude of the carrier.

Given the SMC properties concerning response speed and robustness to external disturbances, considering the system dynamics in (17), a SM controller is designed. From the phase canonical model (18), it can be seen that the controlled state variables $i_d$ and $i_q$ have a relative degree of one. In this way, sliding surfaces suitable to control variables $i_d$ and $i_q$, can be made directly proportional to the state variable feedback errors. The feedback errors are defined as the difference between current references $i_a^*, i_b^*, i_c^*$ and the actual currents, where all of them are derived from their respective d-q components.

The following sliding surfaces should be zero after reaching sliding mode:

$$s_j(e_{ik},t) = i_k^* - i_k = 0 \tag{21}$$

Applying equation (21)

$$s_a(e_{ia},t) = i_a^* - i_a = 0 \tag{22}$$

$$s_b(e_{ib},t) = i_b^* - i_b = 0 \tag{23}$$

$$s_c(e_{ic},t) = i_c^* - i_c = 0 \tag{24}$$

The control strategy must guarantee that the system trajectory moves towards and stays on the sliding surface from any initial condition. In order to achieve this strategy, the following stability condition must be achieved.

$$S_k(e_{ik},t)S_k(e_{ik},t) < 0 \tag{25}$$

Accordingly the switching law is selected as

$$S_a(e_{ia},t) > 0 \Rightarrow S_k(e_{ia},t) < 0 \Rightarrow i_a < i_a^* \tag{26}$$

and $$S_a(e_{ia},t) < 0 \Rightarrow S_k(e_{ia},t) > 0 \Rightarrow i_a > i_a^* \tag{27}$$

A similar procedure is used for the $i_b$ and $i_c$ current error. The current control errors will be quantized using two hysteresis comparators. To improve the performance of SMC, the present work develops a systematic adaptive procedure to calculate the band of the hysteresis [27] comparators.

*Adaptive HB calculation for SMC*

The calculation of hysteresis band is accomplished by considering a simple case with purely inductive load. The current reaches the upper and lower hysteresis band following Fig. 9 which, in turn, yields the voltage-current relationship as given by (28) and (29).

$$L\frac{di_a^+}{dt} = V_{dc} \tag{28}$$

$$L\frac{di_a^-}{dt} = -V_{dc} \tag{29}$$

Adding equation (28) and (29)

$$L\frac{di_a^+}{dt} + L\frac{di_a^-}{dt} = 0 \tag{30}$$

From the geometry of Fig. 9, it can be found

$$t_1\frac{di_a^+}{dt} - t_1\frac{di_a^*}{dt} = 2HB \tag{31}$$

$$t_2\frac{di_a^-}{dt} - t_2\frac{di_a^*}{dt} = -2HB \tag{32}$$

$$t_1 + t_2 = T_{sw} = \frac{1}{f_{sw}} \tag{33}$$

Where $t_1$ and $t_2$ are the respective switching intervals, and $f_{sw}$ is the modulation frequency. Adding (31) and (32), and substituting (33) therein,

$$t_1\frac{di_a^+}{dt} + t_2\frac{di_a^-}{dt} - \frac{1}{f_{sw}}\frac{di_a^*}{dt} = 0 \tag{34}$$

Further, subtracting (32) from (31), one obtains

$$4HB = t_1\frac{di_a^+}{dt} - t_2\frac{di_a^-}{dt} - (t_1 - t_2)\frac{di_a^*}{dt} \tag{35}$$

Now, using (30), (34) and (35) it can be found that

$$4HB = \frac{1}{f_{sw}}\left[\frac{di_a^+}{dt} - \frac{\left(\frac{di_a^*}{dt}\right)^2}{\frac{di_a^+}{dt}}\right] \tag{36}$$

Let $\frac{di_a^*}{dt}$ be denoted by *m*, then (36) can be rewritten as

$$HB = \frac{0.25V_{dc}}{Lf_{sw}}\left[1 - \frac{(mL)^2}{V_{dc}^2}\right] \tag{37}$$

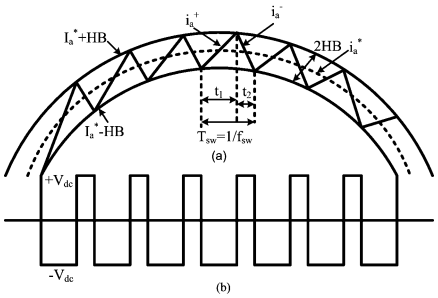


Fig. 9. Time-domain representation of two level hysteresis current controls: (a) current waveforms with hysteresis control, and (b) Voltage source CTLI ac terminal voltage



2168-6777 (c) 2015 IEEE. Personal use is permitted, but republication/redistribution requires IEEE permission. See http://www.ieee.org/publications_standards/publications/rights/index.html for more information.

$$\Rightarrow HB = \frac{0.25V_{dc}}{Lf_{sw(max.)}} \quad (38)$$

This adaptive HB calculation technique is used to improve the PWM performances.

## III. System Configuration

The CTLI topology based photovoltaic (PV) system is depicted in Fig. 1. The open-end winding of a three-phase transformer low-voltage (LV) side is connected between the two inverters. The secondary is directly connected to the distribution grid. The transformer parameters are taken as shown in the Table I [9], which is drawing sinusoidal current from the voltage waveform, as shown later in the result section.

The considered solar irradiance deviation (in percentage) from the initial normal Indian irradiance level is shown in Fig. 10. At time 0.3 s, the solar irradiance decreases and the deviation provided is -17.133 %, and at time 0.6 s, solar radiance is brought back to the rated value. At the time 0.9 s, solar irradiance increases by 17.133 % and then at the time 1.2 s it is brought back to the rated value.

## IV. Results of the Proposed SMC Scheme

The complete grid-connected photovoltaic (PV) system, based on the CTLI, has been simulated in the MATLAB / Simulink environment. The active and reactive power deliveries in response to the variations of solar level are shown in the following subsections.

### *A. Active power variation for two switching schemes*

Fig. 11 (a) shows the output voltage of the voltage source CTLI when using the two-level switching scheme. From this figure, it is possible to verify the multilevel operation of this power converter with the proposed controller. Fig. 11 (b) shows the three-phase output currents of the CTLI. The current is analyzed for harmonic contents and its Fourier spectrum is given in Fig. 11 (c). The voltage ($e_a$, $e_b$, and $e_c$) is applied across the low-voltage (LV) side of the transformer.

The active power supplied by the converters, in the considered reference frame, is found to be directly proportional to the magnitude of $i_d$ (as $V_d$ in the (39) is constant).

TABLE I
TRANSFORMER PARAMETERS

| S. No. | PARAMETER | Value |
|---|---|---|
| 1. | Secondary phase voltage (rms) | 400 V |
| 2. | Primary phase voltage (rms) | 48 V |
| 3. | Frequency | 50 Hz |
| 4. | Power | 2.5 KVA |
| 5. | Transformer leakage inductance, L | 13 % |
| 6. | Transformer resistance | 3 % |

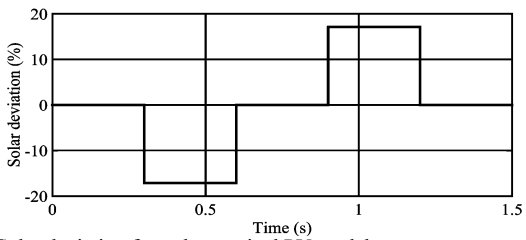


Fig.10. Solar deviation from the nominal PV model

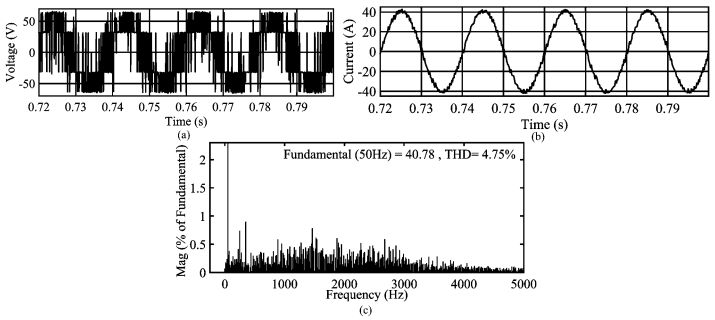


Fig.11.Voltage source CTLI: (a) output voltage of CTLI, (b) CTLI output current ($I_a$), and (c) Harmonic spectrum of output current ($I_a$) for scheme-I

$$P = \frac{3}{2} i_d V_d \quad (39)$$

The solar irradiance at the both inverters connected PV panels is reduced by 17.133 % at 0.3 s. This variation in input is reflected through the reduction in the direct axis component of the inverter output current $i_d$ by 27.64 %, in a step. It is going to 3.618 A from the initial value of 5 A. The $i_q$ is kept constant at zero to ensure no reactive power exchange with the photovoltaic (PV) system. This ensures maximum utilization of the system.

On the other hand, at time 0.3 s, the grid direct-axis current increases by same amount keeping the load current constant. The direct axis and quadrature axis current responses for inverter, grid and load are, respectively, shown in Fig. 12 (a) and 12 (b).

The total dc-link voltage of the inverters suffers a sudden undershoot, and goes back to 96 V within 0.06 s and remains steady at 96 V. The dc voltage changes as shown in Fig. 12 (c). At 0.6 s, the solar irradiance at the inverters is returned to its previous value. The total dc-link voltage of the inverter undergoes an overshoot at 0.9 s in response to the increment in solar irradiance level by 17.133 %. Here the controller successfully brings the voltage back to 96 V within 0.04 s.

The direct axis current component of the inverter, load and grid are found to accommodate this increment successfully.

The increase in irradiance is withdrawn at 1.2 s. In this case, the inverter dc-link voltages experiences a sudden change, however, finally returns to its steady value 96 V. It is interesting to note that due to variation in solar irradiance in inverters, the load direct axis current is constant 61.56 A.

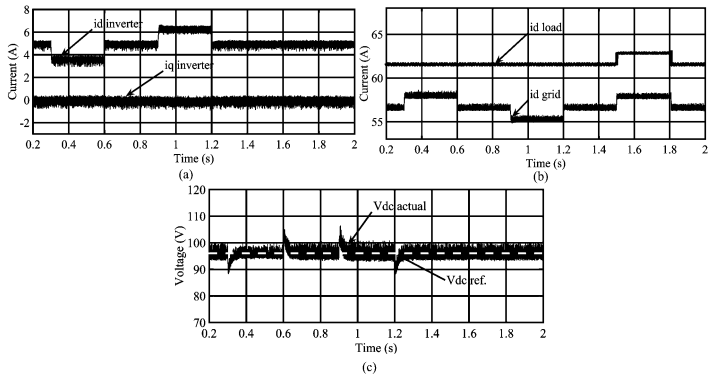


Fig. 12. Grid connected PV system: (a) direct axis and quadrature axis inverter current, (b) direct axis grid and load current, and (c) dc-link voltage for scheme-I



2168-6777 (c) 2015 IEEE. Personal use is permitted, but republication/redistribution requires IEEE permission. See http://www.ieee.org/publications_standards/publications/rights/index.html for more information.

This article has been accepted for publication in a future issue of this journal, but has not been fully edited. Content may change prior to final publication. Citation information: DOI 10.1109/JESTPE.2015.2497900, IEEE Journal of Emerging and Selected Topics in Power Electronics



At time 1.5 s, the load increase by 50 % rated load in a step. Considering the solar irradiance level to be constant the increment in demand is supported by the grid only. The total dc-link voltage suffers no disturbance because of this load change and maximum power delivery from the solar panels is found unaltered.

### B. *Active power variation for forced switching schemes*

Fig. 13 (a) shows the output voltage of the voltage source CTLI while using the "Forced switching" based SM control. Fig. 13 (b) shows the three-phase output currents of the CTLI with the small current ripple. The current is analyzed for harmonic contents and its Fourier spectrum is given in Fig. 13 (c). The THD is coming much lower than the previous scheme.

The solar irradiance is varied in the same manner as it was varied in the earlier scheme. The d-q axis currents for the inverter, load and grid are shown in Fig. 14. The changes in the total dc-link voltage of the two inverters is shown in Fig. 14 (c). The operation is found to supply varying active power and no reactive power, ensuring maximum utilization of the system.

In this switching scheme, also the load increases by 50 % rated load at time 1.5 s. Considering the solar irradiance level to be constant the increment in demand is supported by the grid only. The total dc-link voltage suffers no disturbance because of this load change and maximum power delivery from the solar panels are found undisturbed like the earlier switching scheme. The operation of the controller for the two considered schemes is then tested in the absence of solar irradiance.

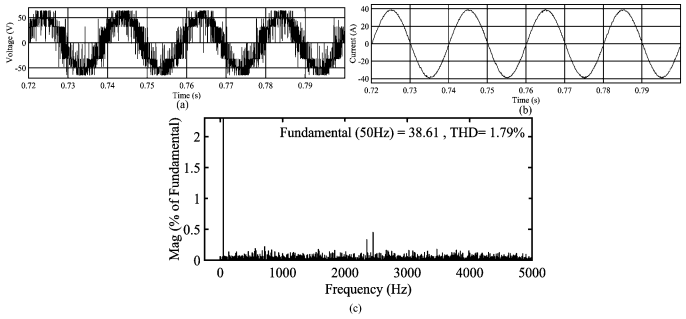


Fig. 13.Voltage source CTLI: (a) output voltage of CTLI, (b) CTLI output current ($I_a$), and (c) Harmonic spectrum of output current ($I_a$) for scheme-II

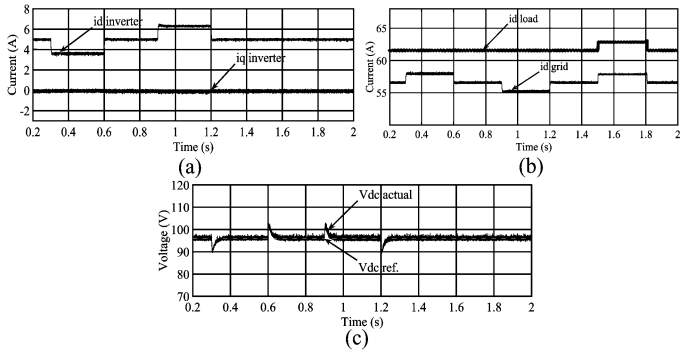


Fig. 14. Grid connected PV system: (a) direct axis and quadrature axis inverter current, (b) direct axis grid andload current, and (c) dc-link voltage for forced switching scheme

### C. *Operation as Distribution STATCOM*

The proposed control scheme enables the PV systems to work in the distribution STATCOM mode, in the absence of solar irradiance, and improves power quality (PQ). The reactive power is expressed in d-q frames can be found as

$$Q = -\frac{3}{2}\left(i_q V_d\right) \tag{40}$$

The reference value for $i_q$ is provided to supply reactive power through an algorithm. In this case, the lagging reactive power supply is increased by 1700 VA in a step, in the absence of solar irradiance. The command is given at 2.5 s in the simulation. The effect, for scheme-I, is shown in Fig. 15.

The $i_q$ is shown to reach the required level of -3.5 A to supply the reactive power. The $i_d$ is found to be zero signifying the fact that no active power is being supplied in the absence of solar power.

Similar operation is tested with the switching scheme-II. The effect, for scheme-II, is shown in Fig. 16. The $i_q$ is shown to reach the required level of -3.5 A to supply the reactive power similarly. However, due to a sudden change in reactive power supply, the capacitors draw some currents from the grid and the losses increase, with an increase in the current supplied by the grid. It is found that the $i_d$ takes 5 ms to be stable. During this operation, the total dc-link voltage is maintained at 96 V after undergoing through some transients, which is as shown in Fig. 15 (c). It takes 4 ms to get back to its reference values 96 V. The instantaneous change in the capacitor voltage happens due to sudden power demand in the distribution STATCOM mode. The effect of a change in reactive power reference is not affecting the dc-link voltage in steady state because of the same dc-link voltage controller.

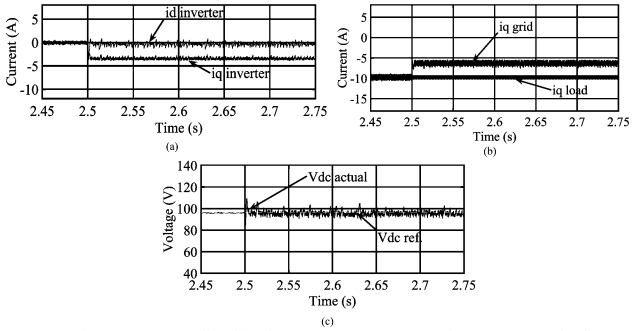


Fig. 15.Voltage source distribution STATCOM mode: (a)d-q axis inverter current, (b) grid and load q-axis current, and (c) dc-link voltage for two level switching scheme

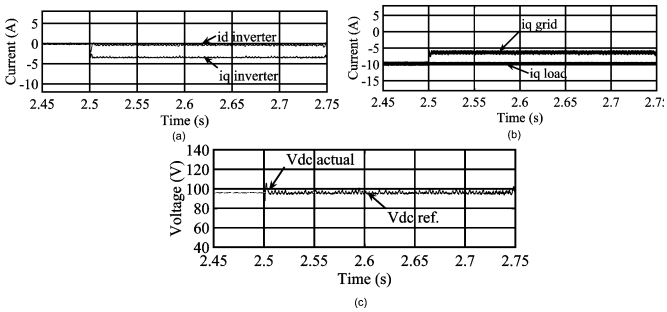


Fig. 16.Voltage source distribution STATCOM mode: (a) d-q axis inverter current,(b) grid and load q-axis current, and (c) dc-link voltage for forced switching scheme



2168-6777 (c) 2015 IEEE. Personal use is permitted, but republication/redistribution requires IEEE permission. See http://www.ieee.org/publications_standards/publications/rights/index.html for more information.

The controller actually maintains the dc-link voltage by balancing the power flow across the capacitor for both the schemes. Hence, it can be mentioned that both the schemes are effective to operate as distribution STATCOM in the absence of solar irradiance.

### *D. Experimental Results*

The CTLI based system is implemented in real time to supply stand-alone balanced load (6 mH and 200 Ω per phase) and results are verified by simulation results. The experimental scheme, using dSPACE1104 with two inverters, is presented in Fig. 17. The equipments, used to prepare the prototype, are mentioned in Table II.

The system operates with the SMC to keep the total voltage of the inverters fixed at the desired level. Here the dc voltages of each inverter is taken as 48 V and hence the total 96 V has to be maintained. The simulation and experimental results are shown in Fig. 18 and Fig. 19.

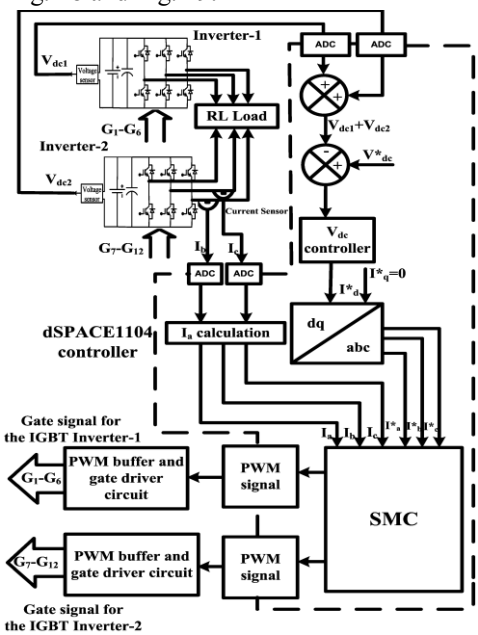


Fig.17. Experimental scheme to implementation sliding mode control (SMC) in real-time

TABLE II
UTILISED COMPONENTS AND PARAMETERS OF PROTOTYPE

| S. No. | PARAMETER | Value |
|---|---|---|
| | **Solar module (two no. for two inverters)** | SYNERGY SOLAR Synergy Electric Pvt. Ltd. (SPEL100) |
| 1. | Open circuit voltage | 80 V |
| 2. | Peak power (of each module) | 400 Wp |
| 3. | Short circuit current | 6.42 A |
| | **Inverter (two numbers)** | SEMIKRON-MDB6U220/300-30F+MDB6CI400/220-27F |
| 4. | Switching frequency | 1000 HZ |
| 5. | Dc-link($V_{dc}$) of each inverter | 48 V |
| 6. | Inverter Switch | IGBT (SKM75GB123D) |
| 7. | Capacitor | 1650 µF/450 V |
| | **Transformer** | |
| 8. | Primary phase voltage (rms) | 48 V |
| 9. | Secondary phase voltage (rms) | 230 V |
| 10. | Frequency | 50 HZ |
| 11. | Leakage inductance, L | 9 % |
| 12. | Resistance, R | 13 % |
| | **Load** | 3-ϕ, 240 V/phase ,10 A |
| 13. | Resistance | 200 Ω |
| 14 | Inductance | 6 mH |

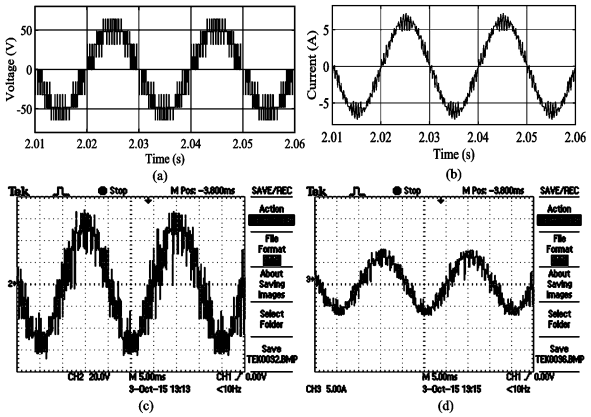


Fig.18. Simulated Inverter outputs (a) line to line voltage, (b) line current, and Experimental Inverter outputs (c) line to line voltage, and (d) line current

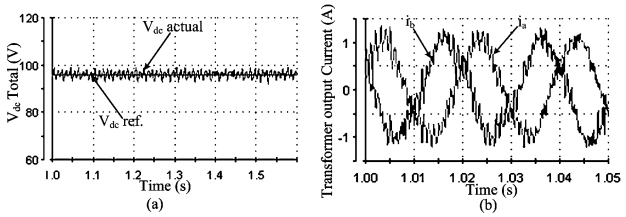


Fig.19. Experimental Results at steady state operation: (a) total dc voltage of two inverters, and (b) transformer output current for two phases

The steady state voltage and current of the experimental system are found to be exactly following the simulation counterparts in Fig. 18. The simulation results are presented in Fig 18 (a) and Fig 18 (b). The experimental inverter output voltage and current are shown in Fig 18 (c) and Fig. 18 (d). The experimental results are exactly following the theoretical predictions. The total voltage is found to be maintained at 96 V as shown in Fig. 19 (a). The transformer output current for two phases are shown in Fig. 19 (b).

## V. CONCLUSIONS

The present work employs a novel and robust SM controller for CTLI based grid connected system. Here the performance of the CTLI is found out to be satisfactory for two different control schemes of SMC. The scheme-I and scheme–II, respectively, consider hysteresis modulation and zero average current error technique to produce the gate signals. Both of the active and the reactive power delivery, in the presence and absence of solar irradiance, are found to be achieved successfully. The controller is shown to extract maximum power from the solar PV modules by maintaining the dc-link voltage at the desired level for both the schemes. The performances under deviations in the input power to the inverters, due to changes in the availability of the solar irradiance, and under 50% increment in load, are found to be satisfactory in nature. The THD of the grid-connected PV system has been studied and found to be considerably within the limit. It is interesting to note that in the absence of solar irradiance, both the control schemes acting distribution STATCOM mode supplying reactive power to the grid, maintaining the dc-link voltage level as well. This ensures the utilization of the PV system for both active and reactive power delivery with the proposed SM controller. The SMC is implemented successfully for the PV based power supply



2168-6777 (c) 2015 IEEE. Personal use is permitted, but republication/redistribution requires IEEE permission. See http://www.ieee.org/publications_standards/publications/rights/index.html for more information.

scheme in real time through dSPACE 1104. The experimental results closely match with the simulation results in the considered situation, which describes the efficacy of the proposed controller.

## REFERENCES


[1] J.M. Carrasco, L.G. Franquelo, J.T. Bialasiewicz, E. Galván, R.C.P. Guisado, M.Á.M. Prats, J.I. León, and N.M. Alfonso, "Power-electronic systems for the grid integration of renewable energy sources: A survey," *IEEE Trans. Ind. Electron.* vol. 53, no. 4, pp. 1002-1016, Aug. 2006.

[2] B. Sahan, S.V. Araujo, C. Noding, and P. Zacharias, "Comparative Evaluation of Three-Phase Current Source Inverters for Grid Interfacing of Distributed and Renewable Energy Systems" *IEEE Trans. Power Electron.*, Vol. 26, no. 8, pp. 2304 - 2318, 06 Dec. 2010.

[3] S. Kouro, J.I.Leon, D.Vinnikov and L.G. Franquelo, "Grid-Connected Photovoltaic Systems an overview of Recent Research and Emerging PV Converter Technology," *IEEE Ind. Electron. Mag.,* vol. -9, no-1, pp.-47-61, 19 Mar.2015.

[4] F. Blaabjerg, Z. Chen, and S. B. Kjaer, "Power electronics as efficient interface in dispersed power generation systems," *IEEE Trans. Power Electron.*, vol. 19, no. 5, pp. 1184–1194, Sept.2004.

[5] V.F. Pires, J.F. Martins, and C. Hao, "Dual-inverter for grid-connected photovoltaic system: Modeling and sliding mode control," *Elsevier Solar Energy,* vol. 86, no.7, pp. 2106-2115, July 2012.

[6] A. Edpuganti, and A.K. Rathore, "New Optimal Pulse width Modulation for Single DC-Link Dual-Inverter Fed Open-End Stator Winding Induction Motor Drive," *IEEE Trans. Power Electronics,* Vol.30, no. 8, pp.4386 - 4393, Aug. 2015.

[7] S.Kouro, J.Pou, L.G.Franquelo, B.Wu, J.Rodriguez, M.A.Pérez, and J.I.Leon, "Recent Advances and Industrial Applications of Multilevel Converters," *IEEE Trans. Ind. Electron..,* Vol.57, no. 8, pp.2553-2580, Aug.2010.

[8] J. Rodriguez, J.-S. Lai, and F. Z. Peng, "Multilevel inverters: A survey of topologies, controls, and applications," *IEEE Trans. Ind. Electron.*, vol. 49, no. 4, pp. 724–738, Aug. 2002

[9] N.N.V.S. Babu, D.A. Rao and B.G. Fernandes, "Asymmetrical DC Link Voltage Balance of a Cascaded Two Level inverter Based STATCOM", *TENCON 2010-2010 IEEE Region 10 Conference*, 21-24 Nov. 2010, Fukuoka, pp. 483–488.

[10] M. Malinowski, K. Gopakumar, J. Rodriguez, and M .A. Pérez, "A Survey on Cascaded Multilevel Inverters," *IEEE Trans. Ind. Electron.*, Vol. 57, no. 7, pp. 2197-2206, July 2010.

[11] N.N.V.S. Babu, and B.G. Fernandes, "Cascaded Two-Level Inverter-Based Multilevel STATCOM for High-Power Applications," *IEEE Trans. Power Del.*, vol. 29, no. 3, pp.993-1001, June 2014.

[12] N. Kumar, T.K. Saha, and J. Dey, "Cascaded Two Level Inverter Based Grid Connected Photovoltaic System: Modeling and Control," *IEEE International Conference on Industrial Technology (ICIT)*, Feb.26-Mar.1, 2014, Busan, Korea, pp. 468-473.

[13] G. Grandi, C. Rossi, D. Ostojic, and D. Casadei, "A New Multilevel Conversion Structure for Grid-Connected PV Applications", *IEEE Trans. Ind. Electron.*, vol. 56, no. 11, pp.4416-4426,Nov. 2009

[14] B.P. McGrath, and D.G. Holmes, "Multicarrier PWM strategies for multilevel inverters," *IEEE Trans. Ind. Electron.,* Vol.49, no. 4, pp. 858 - 867, Aug. 2002.

[15] S. C. Tan, Y.M. Lai and C. K. Tse, "Sliding Mode Control of Switching Power Converters Techniques and Implementation" London, U.K: *Taylor and Francis,* 2012.

[16] K.D. Young, V.I. Utkin, U. Ozguner, "A control engineer's guide to sliding mode control," *IEEE Trans. Control Syst. Technol.,* Vol.7, no. 3, pp. 328-342, May 1999.

[17] J. Y. Hung, W. Gao, and J.C. Hung, "Variable structure control: A survey," *IEEE Trans. Ind. Electron.*, Vol. 40, no. 1, pp. 2-22, Feb. 1993.

[18] V. Utkin, J. Guldner, and J. Shi, "*Sliding Mode Control in Electromechanical Systems,* "London, U.K: *Taylor and Francis,* 2009.

[19] V. I. Utkin, "Variable structure systems with sliding mode," *IEEE Trans. Autom. Control*, vol. 22, no.2, pp. 212-222, April 1977

[20] R. Gupta, and A. Ghosh "Frequency-Domain Characterization of Sliding Mode Control of an Inverter Used in DSTATCOM Application," *IEEE Trans. Circuits Syst. I, Reg. Papers*, Vol. 53, no. 3, pp. 662-676, March 2006.

[21] K. K. Mohaptra, K. Gopakumar, and V. T. Somasekhar, and L. Umanand, "A harmonic elimination and suppression scheme for an open-end winding induction motor drive," *IEEE Trans. Ind. Electron..*, vol. 50, no. 6, pp. 1187-1198,Dec. 2003

[22] M.G. Villalva, J.R. Gazoli, and E.R. Filho, "Comprehensive Approach to Modeling and Simulation of Photovoltaic Arrays," *IEEE Trans. Power Electron.*, vol. 24, no. 5, pp.1198-1208, May 2009.

[23] J. A. Gow, and C.D. Manning, "Development of a photovoltaic array model for use in power-electronics simulation studies," *IEE Proc. Electr. Power Appl.,* vol. 146, no.2, pp.193-200, March 1999.

[24] S. A. Rahman1, R. K. Varma1 and T. Vanderheide, "Generalised model of a photovoltaic panel" *IET Renewable Power Generation*, Vol. 8, Iss. 3, pp.-217-229,August 2013

[25] W. Xiao, W.G. Dunford and A. Cape "A novel modeling method for photovoltaic cells,"*35th IEEE Power Electronics Specialist Conf.*, 2004, pp. 1950 –1956.

[26] J. A. Gow and C. D. Manning, "Development of a model for photovoltaic arrays suitable for use in simulation studies of solar energy conversion systems*," 6th Int. Conf. Power Electron. Variable Speed Drives,* 1996, pp. 69–74.

[27] B.K. Bose, "An adaptive hysteresis-band current control technique of a voltage-fed PWM inverter for machine drive system, " *IEEE Trans. Ind. Electron.*, Vol.37, no.5, pp.402-408, Oct. 1990.

[28] J. F. Silva, "Sliding mode control of voltage sourced boost-type reversible rectifiers," *IEEE ISIE'97*, July 1997, vol. 2, pp. 329–334.

[29] J. F. Silva, "Sliding-Mode Control of Boost-Type Unity-Power-Factor PWM Rectifiers Sliding," *IEEE Trans. Ind. Electron*., vol. 46, no. 3, June 1999.

[30] Ben Azza H., Zaidi N., Jemli M. and Boussak, M., "Development and Experimental Evaluation of a Sensorless Speed Control of SPIM Using Adaptive Sliding Mode-MRAS Strategy," *IEEE Journal of Emerging and Selected Topics in Power Electronics*, , vol.2, no.2, pp. 319-328, Jun. 2014


**Nayan Kumar** He is currently working towards the Ph.D. degree in the Department of Electrical Engineering, National Institute of Technology, Durgapur, India. His research interests are power-electronic and its applications and renewable energy.

**Tapas Kumar Saha ( M'09)** received the B.E., M.E.E., and Ph.D. in 1997, 1999, and in 2009 respectively. He is currently an Associate Professor in the Department of Electrical Engineering, National Institute of Technology Durgapur, India. His current research interests are machine drives, power electronics, renewable energy and the grid integrated distributed generations

**Jayati Dey ( M'09)** received the B.E.E., M.E., and Ph.D. in 2000, 2003, and in 2007 respectively. She is currently an Assistant Professor in the Department of Electrical Engineering, National Institute of Technology Durgapur, India. Her research interests are periodic compensation, switching power converters, robotics and mechatronics with special interest in robust control.



2168-6777 (c) 2015 IEEE. Personal use is permitted, but republication/redistribution requires IEEE permission. See http://www.ieee.org/publications_standards/publications/rights/index.html for more information.